



Fire Performance of Corroded Reinforced Concrete Columns

Shashank Chandra * and *Umesh Kumar Sharma* , Department of Civil Engineering, IIT Roorkee, Roorkee, India

Mark Green , Department of Civil Engineering, Queen's University, Kingston, ON, Canada

John Gales , Department of Civil Engineering, York' University, Toronto, ON, Canada

Pradeep Bhargava , Department of Civil Engineering, IIT Roorkee, Roorkee, India

Received: 23 March 2023/**Accepted:** 19 July 2023/**Published online:** 10 August 2023

Abstract. The present standards for finding the fire ratings of reinforced concrete (RC) columns are restricted to pristine elements, as the age or corrosion-related deteriorations are yet to be addressed. An experimental investigation was conducted to examine the impact of corrosion on the fire performance of reinforced concrete columns. This investigation studied two normal-strength concrete (NSC) and two high-strength concrete (HSC) RC columns. Out of these four columns, one NSC and one HSC column were corroded by a specifically designed accelerated corrosion setup for the target corrosion of 20%, while the remaining columns were the control specimens and were kept uncorroded. After completing the desired exposure time for the accelerated corrosion, both columns and their companion non-corroded columns were tested in a fire furnace simulating the standard ISO-834 fire. The experimental results showed that corrosion has a significant influence on the fire performance of the RC columns. The result indicates that the fire rating of the corroded HSC column drops considerably. Nevertheless, there exists a subtle enhancement in the behavior of the corroded NSC column when exposed to fire, indicating the need for further research in this regard. The effects of corrosion cracks and spalling on the fire resistance of the corroded RC columns were also noted in this study. This research will enable the design of new reinforced concrete columns for better fire performance despite corrosion-related deteriorations.

Keywords: Corrosion in structures, Age-related deteriorations, Fire ratings, Corrosion-temperatures interactions, Corroded reinforced concrete columns

List of Symbols

f_{ck}	Characteristics compressive strength of concrete
A_c	Area of concrete
f_y	Yield strength of longitudinal reinforcement
A_{sc}	Area of longitudinal reinforcement
f'_c	Compressive strength of concrete cube of $150 \times 150 \times 150$ (mm) size.
P	Initially applied load over the column during fire testing

*Correspondence should be addressed to: Shashank Chandra, E-mail: schandra1@ce.iitr.ac.in



1. Introduction

Reinforced concrete (RC) structures in humid and coastal regions are susceptible to corrosion-related deterioration. Corrosion is an electrochemical reduction process in which the reinforcements' sectional area is reduced [1]. Also, the corrosion products formed through this process contain significantly more volume than their parent ones, producing a high hoop stress over the cover concrete and the cracks are observed over the faces of the RC member [2]. These cracks act as a convenient passage for the further transfer of external deteriorating agents into the concrete in a more progressive manner. The bond strength between the reinforcement and concrete of the RC element is significantly compromised due to the corrosion process [3–5]. Finding the effect of corrosion on the structural performance of RC elements has been the theme of investigators in the past [6–10].

In addition, unintentional fire also poses a severe threat to the infrastructure. In 2016, 96,800 non-residential fire incidents were recorded by the U.S. Fire Administration (USFA), resulting in a \$2 billion loss [11]. However, the concrete has excellent thermal resistance due to its low thermal conduction properties; still, at high temperatures, various physical and chemical changes occur in the microstructure of the concrete [12–15]. These changes significantly affect the mechanical behaviour of the concrete. The load transfer mechanism of RC members at elevated temperatures also gets compromised due to the weakening of the bond between the concrete and steel [16, 17]. Fire safety of infrastructure is handled by incorporating various active and passive fire protection measures. The different active fire protection measures like sprinklers, fire alarms, smoke detectors, fire hydrant systems, fire suppression systems etc., come into the role during a fire incident. Passive fire protection is the integral fire protection property of a material. In a fire, the RC structural members' internal fire protection ability is the last line of defense when these active fire protection systems fail. This integral or passive fire protection is called fire resistance or fire rating, a standard tool to quantify the fire safety ability of the structural elements. Fire resistance or fire rating is defined as the fire duration (in minutes or hours) under which a structural part will not lose its load-bearing capacity, stability and integrity [18]. For a load-bearing element like a beam and column, the structural component is assumed to be failed when its functional criteria, i.e., load-bearing capacity, will no longer provide resistance against fire. A column is the main load-bearing element in a structure, and thus it must sustain its load-carrying capacity during an event of a fire. The influence of elevated temperatures on the structural behavior of RC columns has also been the theme of investigators in the past [19–23]. Simple calculation methods to calculate the fire ratings of RC columns have also been developed, as given in Eurocode 2 [24] and the Australian code [25].

Much research data is available to quantify the risk imposed by corrosion and fire but in an independent form. It is reasonable to assume that the corroded RC columns might not behave similarly to their non-corroded specimens. The corrosion cracks can cause a rapid increase of heat propagation inside the RC member during the event of a fire. Very few attempts have been carried out in the litera-

ture to quantify the risk of corrosion over the fire performance of RC elements [26–28]. Still, there is no literature available to quantify the risk of corrosion over the fire performance of RC columns. The present study bears significance as it investigates the performance of aged or corroded RC columns when exposed to an event of a fire. This research tries to mimic the behavior of aged or old structures exposed to a fire. The literature that is currently accessible contains a wealth of information regarding the post-corrosion behaviour of reinforced concrete elements as well as their recovery from damage caused by corrosion. When corrosion gets superimposed by exposure to high temperatures, the behaviour of reinforced concrete components is not well described in the literature. The need for a thorough study to quantify the risk of corrosion for the fire resistance of RC columns has been further highlighted by recent field inspections carried out by the authors. To this end, an experimental study was conducted in which four RC columns were cast, corroded and tested in a fire furnace lab facility.

2. Experimental Work

2.1. Casting of RC Column Specimens

Four RC columns were put through fire tests as part of this experimental program, as shown in Table 1. Two columns, C30220C and C30300C, were of normal-strength concrete (NSC) of grade M30 ($f_{ck} = 30 \text{ N/mm}^2$), and the other two column specimens, C60120C and C60500C, were of high-strength concrete (HSC) of grade M60 ($f_{ck} = 60 \text{ N/mm}^2$). The fact should be noted that two of these four RC columns were corroded for the target corrosion of 20%, and the remaining two were non-corroded control RC column specimens. The C30300C and C60500C column specimens were the control specimens for the C30220C and C60120C column specimens, respectively. As shown in Figure 1, all the column specimens were 300 mm × 300 mm in cross-section and 3150 mm in height. At a cover depth of 40 mm, the longitudinal bars of each column specimen were 4 Nos -20 mm and 4 Nos-16 mm. The stirrups and cross ties to tie these longitudinal bars were 8 mm @ 100 mm c/c. Transverse and longitudinal reinforcing elements

Table 1
Summary of Test Specimens

Column designation	Concrete type	Compressive strength (MPa) (f_c)		Targeted Corrosion	Accelerated Corrosion exposure time
		28-day	Test-day		
C30220C	NSC	36	39	20%	70 days
C30300C	NSC			0%	–
C60120C	HSC	67	71	20%	100 days
C60500C	HSC			0%	–

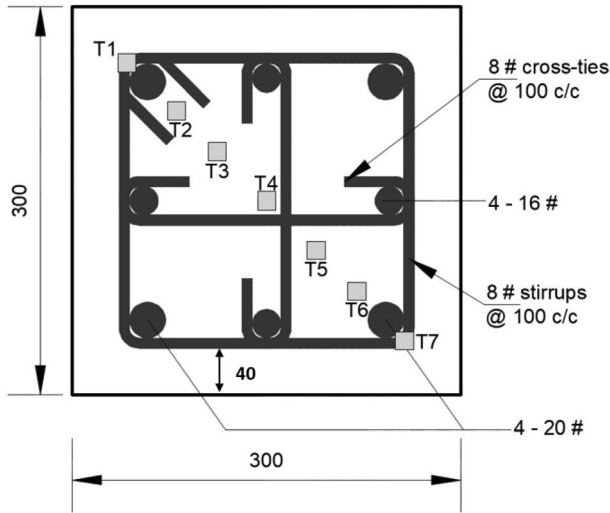


Figure 1. Cross-sectional details of RC column (all dimensions in mm).

had an average yield strength of 492.3 MPa for 8 mm bars, 498.9 MPa for 20 mm bars, and 496.7 MPa for 16 mm bars. As shown in Figures 1 and 2c, seven K-type internal thermocouples of 0.85 thickness (T1 to T7) were installed along the diagonal of the column at three locations along the height of the column (at quarter length from top, quarter length from bottom and mid-section of the fire zone). These internal thermocouples were installed to record the thermal gradients inside the RC column during the fire testing. All four RC columns were cast vertically, as shown in Figure 2a, using the concrete mixer for mixing and the needle pipe vibrator for proper compaction. As the height of the columns was 3.15 m, it was not feasible to pour all of the concrete from the top of the formwork to ensure no concrete segregation. Therefore, a unique window arrangement was made in the formwork at the height of 1.5 m, as shown in Figure 2b. A two-phase casting scheme was adopted during the casting of all the column specimens. In the first phase, the mixed concrete was poured from this window and vibrated from the top of the formwork and in the second phase, the window was closed, and then the concrete pouring and the vibration were done from the top of the formwork. This two-phase scheme of pouring helped to achieve no segregation of concrete. The properties of the materials used for making the concrete are mentioned in Tables 2, 3, 4, 5 and 6. Two batches of concrete were prepared to cast these four RC column specimens. Batch-1 concrete was used for casting NSC columns (C30220C and C30300C), and Batch-2 concrete was used for casting HSC columns (C60120C and C60500C). The mix proportions of these two batches of concrete are mentioned in Table 7. Six standard cubes were also cast along with their respective column, which enabled finding the average compressive strength of the concrete on the 28th day and the day of the column testing in the fire, as mentioned in Table 1. A relative humidity (RH) probe was used to find the relative



Figure 2. (a) The casting of RC columns. (b). Window opening in the formwork. (c). Installation of thermocouples.

**Table 2
Physical Properties of Cement Used in the Casting**

Characteristics	Units	Results obtained	Recommended values as per IS 8112:1989
Blaine's fineness	m ² /kg	258	225 (minimum)
Specific gravity	-	3.14	-
Soundness (Le-Chatelier Test)	mm	3.1	10 (maximum)
Autoclave expansion	%	0.074	0.8 (maximum)
Normal consistency (Percent of cement of weight)	%	27.5	30
Setting Time			
(1) Initial setting time	Minutes	92	30 (minimum)
(2) Final setting time	Minutes	187	600 (maximum)

Table 3
Chemical Composition of OPC-43 Portland Cement Used in the Casting

Oxides	Test Results (%)	Limiting values as prescribed by IS 8112:1989 (%)
Silica (SiO ₂)	21.3	19–24
Alumina (Al ₂ O ₃)	5.21	3–6
Ferric oxide (Fe ₂ O ₃)	3.92	1–4
Sodium oxide (Na ₂ O)	0.29	≤ 0.6
Potassium oxide (K ₂ O)	0.31	–
Calcium oxide (CaO)	62.26	59–64
Magnesia oxide (MgO)	2.41	≤ 6
Sulphuric anhydride (SO ₃)	1.60	≤ 3
Insoluble residue	1.22	≤ 2
Loss on ignition	0.81	≤ 5

Table 4
Physical and Chemical Properties of Micro Silica

Properties	Results obtained
Blaine's finesses (cm ² /gm)	22,000
Specific gravity	2.20
Silicon dioxide (SiO ₂) (%)	92.13
Alumina (Al ₂ O ₃)	0.56
Ferric oxide (Fe ₂ O ₃)	1.10
Sodium oxide (Na ₂ O)	0.42
Potassium oxide (K ₂ O)	0.23
Loss on ignition	1.75

Table 5
Physical Properties of Fine Aggregate

Characteristics	Requirement as per IS 383:1970	Results obtained
Grading	–	Conforming to grading zone II
Fineness modulus	2.0–3.5	2.68
Specific gravity	2.6–2.7	2.61
Density (loose) (kN/m ³)	–	13.7
Water absorption (%)	–	1.18
Moisture content (%)	–	0.35

humidity of the test specimen on the day of the testing. The relative humidity was measured by drilling a hole at a depth of 50 mm. The values of the RH are mentioned in Table 8. It was found that the corroded columns, C30220C and C60120C, had higher relative humidity than their companion non-corroded speci-

Table 6
Physical Properties of Crushed Calcareous Coarse Aggregate

Characteristics	Requirement as per IS 383:1970	Results obtained
Fineness modulus	5.5–8	6.46
Specific gravity	2.6–2.7	2.67
Density (loose) (kN/m ³)	–	15.19
Water absorption (%)	–	0.63
Moisture content (%)	–	Nil

Table 7
Concrete Mix Proportions of Casted RC Column Specimens

	Batch-1	Batch-2
Columns casted	C30220C, C30300C	C60120C, C60500C
Concrete type	NSC	HSC
Cement (kg/m ³)	379	500
Water (kg/m ³)	205	150
Silica fume (kg/m ³)	–	51
Coarse aggregate (kg/m ³)	940	1045
Fine aggregate (kg/m ³)	880	618
Superplasticizer (kg/m ³)	–	5.18
Slump (mm)	71	96

Table 8
Applied Load and Fire Resistance Results of RC Column Specimens

Column specimen	Load Applied (kN)	Fire resistance (minutes)	Relative humidity (%)	Spalling area
C30220C	576	255	74.2	0%
C30300C	576	239	73.2	11.1%
C60120C	925	118	83.5	63.5%
C60500C	925	171	79.2	59.2%

mens, C30300C and C60500C, respectively. This must be because corroded columns were kept in a submerged condition during the accelerated corrosion.

2.2. Accelerated Corrosion of RC Column Specimens

After casting RC column specimens, the specimens were cured using wet gunny bags for 28 days. After that, one (C30220C) of the two NSC columns and one (C60120C) of two HSC columns were installed for accelerated corrosion. These columns were corroded for the central column length of 2.15 m, using a specifi-

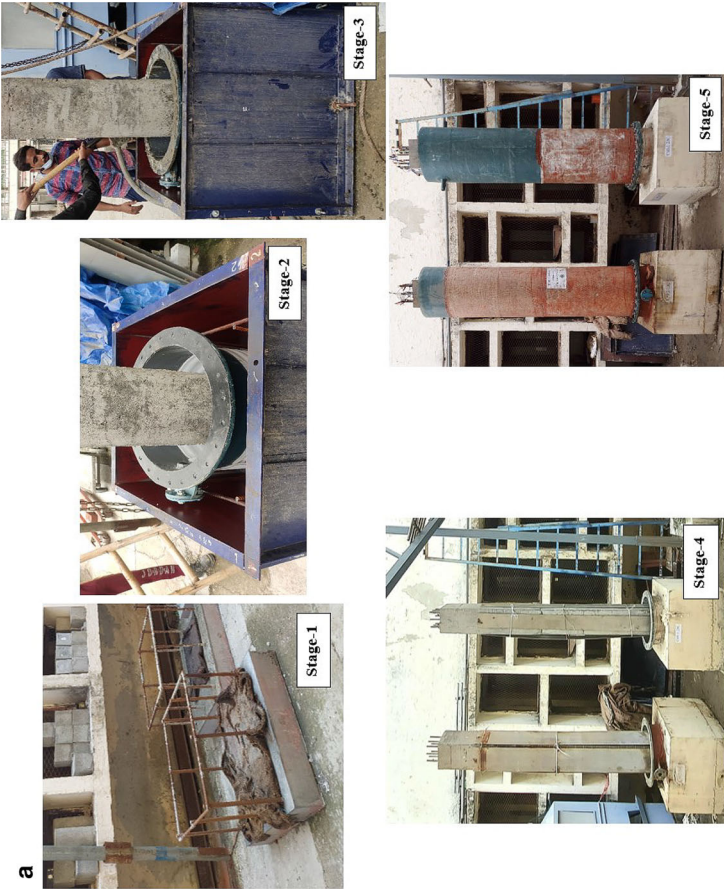


Figure 3. (a) Installation of Accelerated corrosion setup. (b) Schematic of installation of Accelerated corrosion setup (all dimensions in mm).

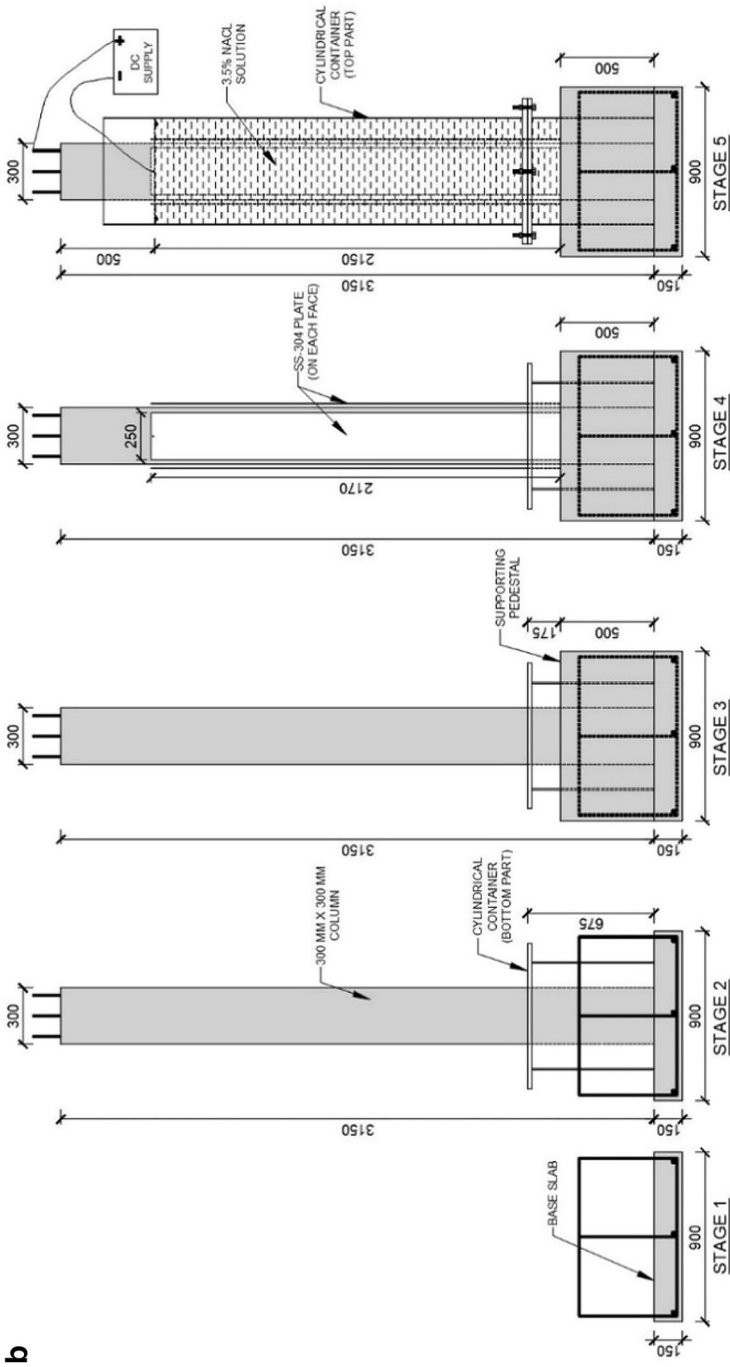


Figure 3. continued.

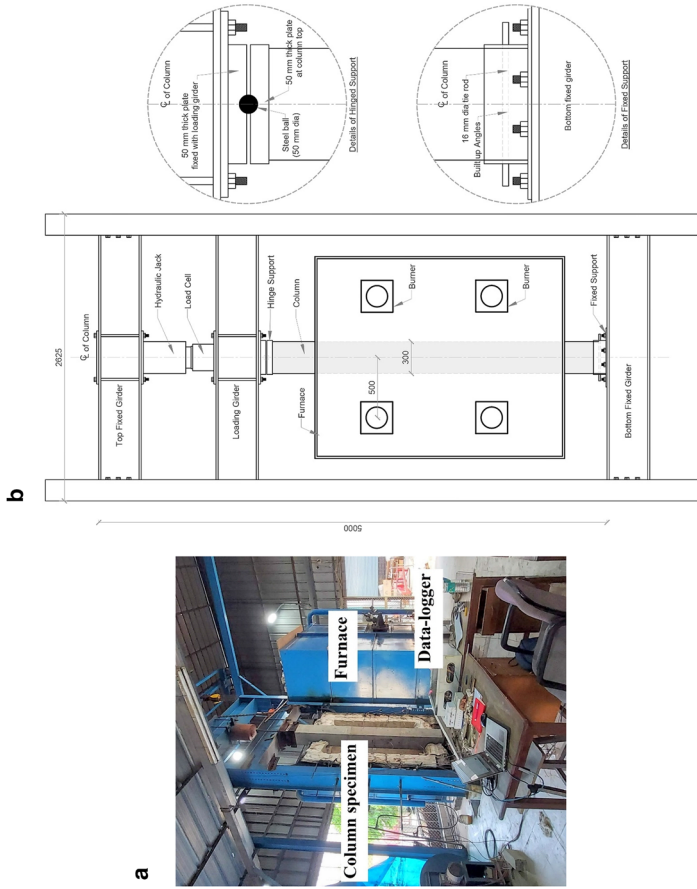


Figure 4. (a) Fire furnace facility. (b) Schematic of fire furnace facility and support conditions during the test (all dimensions in mm).

cally designed corrosion setup using the installation process, as shown in Figure 3a. The schematic of the installation process is also mentioned in Figure 3b. The concept of electrochemical reaction was followed for the accelerated corrosion of these columns; this concept has been reported and validated by several other researchers in the past as well [3–8]. For an electrochemical reaction to happen, there was a need for an electrolyte solution. A 3.5% NaCl solution was used as an electrolyte during the accelerated corrosion. A considerable amount of such NaCl solution was required to submerge the column. For that, specially fabricated non-metallic cylindrical containers were manufactured. This container was made in two parts, a bottom part (560 mm ϕ and 675 mm height) and a top part (560 mm ϕ and 2900 mm height). The process of installation of the accelerated corrosion setup comprised five stages. In stage-1, an RC base slab (900 mm \times 900 mm \times 150 mm) was cast. The reinforcements of this base slab were coming out of the base slab, which acted as the reinforcements for further casting. In stage-2, the RC column and the bottom part of the cylindrical container were kept over such casted base slab. In stage-3, the internal and external castings up to the height of 500 mm were done to make a supporting pedestal. It should be noted here that after stage-3, the bottom 500 mm length of the RC column specimen, along with the bottom cylindrical container, is under this casted supported pedestal. In stage-4, SS-304 plates were attached to the faces of the column. In stage-5, the top cylindrical container was put over the bottom container and fixed using the nut-bolt assemblies. After this, the container was filled with the 3.5% NaCl solution up to a height of 500 mm from the top of the column. Such an arrangement ensured that the central 2.15 m portion of the column was submerged in the electrolyte solution. Then, the SS-304 plates and reinforcements of the column were connected to a specially designed DC supply as cathode and anode, respectively, and the current at the current density of $300\mu\text{A}/\text{cm}^2$ was passed for their respective corrosion exposure time. Such a two-part container assembly enabled periodic monitoring of corrosion activities, as discussed in Sect. 3.3 of this paper.

2.3. Fire Testing of RC Column Specimens

After their respective exposure time, the corroded columns (C30220C and C60120C) and their companion non-corroded columns (C30300C and C60500C) were tested in a fire furnace facility. This furnace (Figures. 4a and b) has fire zone dimensions of 2.175 m height, 1 m width and 1 m depth. The desired ISO-834 fire exposure [29] and load over the RC column can both be applied simultaneously in this furnace. The fire exposure in this furnace is provided by the four diesel burners installed to supply fuel and air. Four MI thermocouples were attached to the furnace to record the average furnace-air temperature during the fire test. Two LVDTs, LVDT-V1 and LVDT-V2, were installed at the top of the column to record the axial deformations of the RC column during the fire test. The lateral deformation of the RC column during the fire test was also recorded using the other LVDTs installed at the side face of the column. During the fire test, the bottom support of the column was kept fixed, and the top support of the column was kept pinned. A tie rod of 16 mm diameter was cast in all the column specimens,

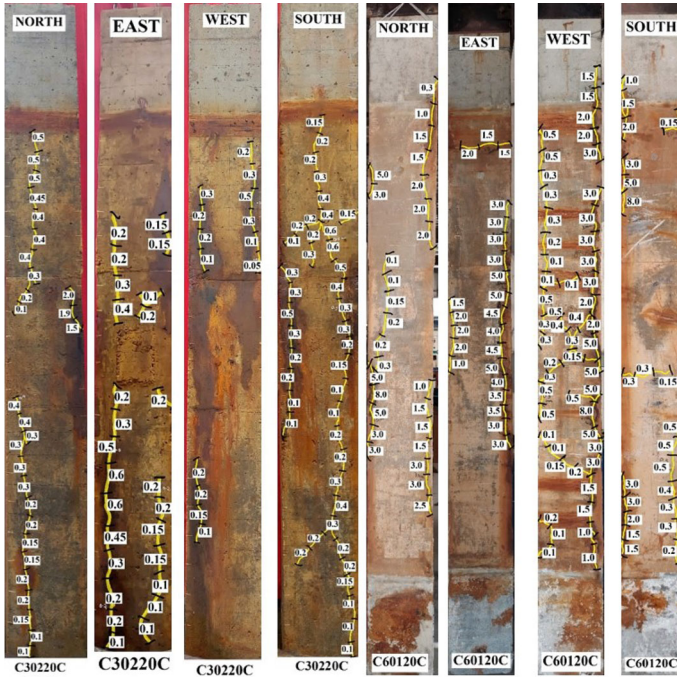


Figure 5. Crack observation (mm) for corroded RC column specimens. Here, C30220C = Corroded NSC; C60120C = Corroded HSC.

which helped to provide fixed support conditions using built-up angles, as shown in Figure 4b. The hydraulic jack was used to apply the load, and a load cell setup was used to measure it. All the columns tested under this study were concentrically loaded, and extra care was taken to match up the center lines of the hydraulic jack and column. Before the test, a steel plate of 50 mm thickness with a special groove that was 20 mm deep was fastened to the top surface of the col-

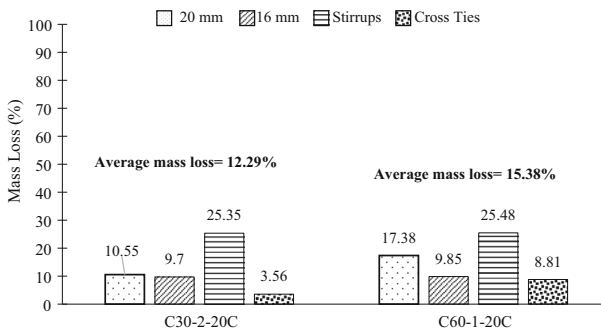


Figure 6. Gravimetric analysis of corroded RC columns. Here, C30-2-20C = Corroded NSC; C60-1-20C = Corroded HSC.

umn. Another similar plate of 50 mm thickness with the same groove arrangement was fixed with the loading girder. The load was applied by putting a 50 mm diameter steel ball inside these grooves, as shown in Figure 4b. As shown in Table 8, the static load (P) applied to the column specimens was 33% of its design load-carrying capability. The design carrying capacity of each column was estimated by the method mentioned in IS-456 [30]. This load was maintained for 30 min before the column was exposed to fire. These instrumentations were linked to a multi-channel data logger to record the pertinent data during the fire tests. The load acting on the column rose in the early fire exposure because of the column's expansion. After further fire exposure, it decreased and returned to the initially applied load (P). Then, the load was tried to maintain at this level until a sudden drop was observed, and the column could no longer sustain the load. The test was terminated at this point, and the column was declared to have failed.

3. Results and Discussions

3.1. Corrosion Exposure Observations after the Accelerated Corrosion

As previously stated, accelerated corrosion was applied to two of the four RC column specimens using a specifically designed setup. After the corrosion period, the corresponding columns were removed from the supporting pedestal and examined for corrosion cracks, as shown in Figure 5, using a crack width meter with a minimum resolution 0.05 mm. Even though similar current densities and exposure conditions were ensured throughout the corrosion process, each specimen's crack patterns varied on each face of the columns. It must be because concrete has a diverse microstructure and is a heterogeneous substance. The cracks ranged in size from 0.1 to 8 mm. Even though longitudinal cracks were the most common, diagonal cracks could also be seen on the faces of the column specimens. It should be observed that the direction of the corrosion cracks mainly indicates the orientation of the corroding reinforcement cage, so longitudinal cracks and diagonal direction cracks indicate corrosion of longitudinal reinforcement and transverse reinforcement, respectively.

Table 9
Monitoring Sessions of HCP Measurements

Column specification	Monitoring sessions	Age of accelerated corrosion
C30220C (Corroded NSC)	Monitoring-0	0th day
	Monitoring-1	40th day
	Monitoring-2	70th day
C60120C (Corroded HSC)	Monitoring-0	0th day
	Monitoring-1	40th day
	Monitoring-2	70th day
	Monitoring-3	100th day

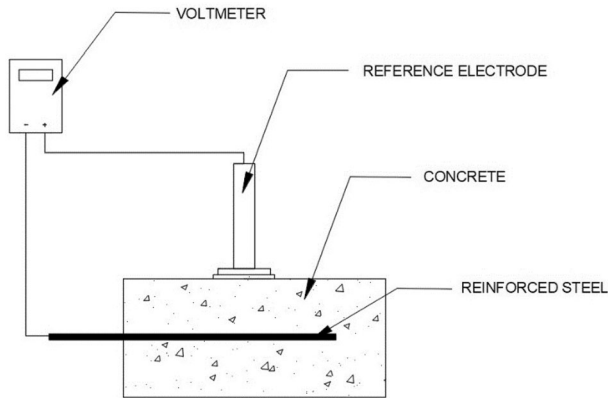


Figure 7. Schematic of Half-cell potential equipment.

3.2. Gravimetric Analysis after Fire Testing

Following the fire test, the corroded specimens were demolished, the reinforcing elements were extracted and cleaned, and their residual weights were calculated to determine the actual mass loss from corrosion using ASTM G1-03 [31] guidelines. The initial weight of the reinforcing elements, before the corrosion exposure, was already noted before the casting of the RC column specimens. This gravimetric analysis is shown in Figure 6. It can be noticed that the NSC column (C30220C), which was put in the accelerated corrosion for 70 days, suffered a mass loss of 12.29%, whereas the HSC column (C60120C), which was placed in the accelerated corrosion exposure for 100 days, suffered the mass loss of 15.38%. Figure 6 also displays the mass loss experienced by individual reinforcing cage components in all specimens' test lengths (2.15 m). It can be noticed that compared to the other components of the reinforcing cage, the stirrups experienced more severe corrosion. The fact that 20 mm longitudinal bars lost more mass than 16 mm bars is also clear from Figure 8. This must be because the 20 mm bars had two faces exposed in the column. The cross ties experienced a minor mass loss; this must be because the reinforcing cage elements close to the core of the concrete are less affected by chloride ingress from the concrete's surface.

3.3. Periodical Half-Cell Potential Measurements During Accelerated Corrosion

Half-cell potential (HCP), which helps in corrosion monitoring, shows the probability of corrosion of the reinforcements embedded inside any concrete element. The configuration of the accelerated corrosion apparatus used in this experimental study allowed for the periodical monitoring of HCPs. To examine the changes in the potential readings, three and four monitoring periods for C30220C and C60120C, respectively, were carried out using Ag/AgCl reference electrode-based half-cell equipment, as shown in Table 9. The schematic of half-cell equipment is shown in Figure 7. The surface preparations and HCP tests were conducted in

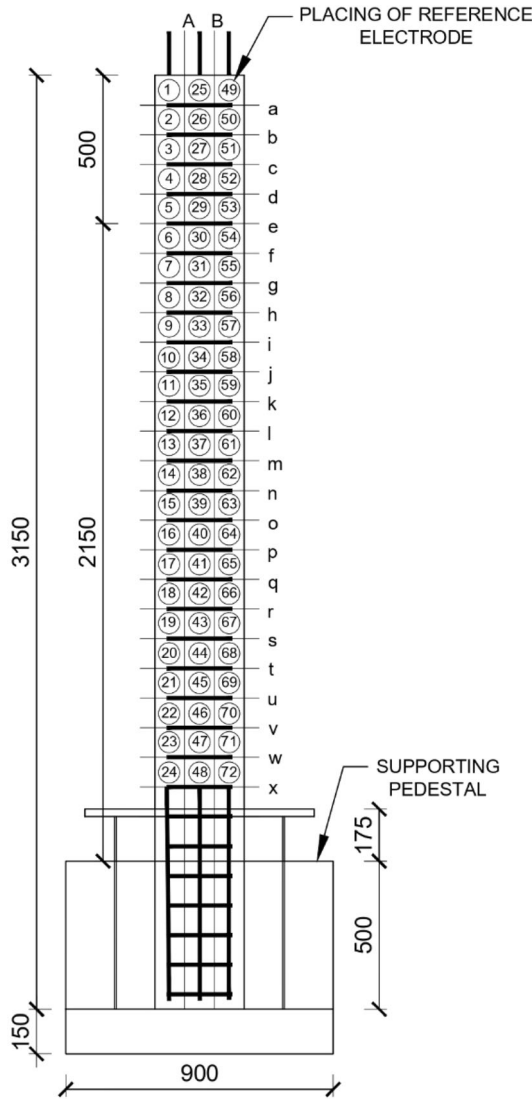


Figure 8. HCP monitoring data points.

accordance with IS 516 (Part 5/Sec 2) [32]. Grid lines were drawn on the column faces using a rebar locator before using this half-cell equipment, as shown in Figure 8. A total of 72 points on each face were identified and considered for HCP monitoring for all the periodically performed monitoring sessions. Four states were grouped based on the different HCP values obtained during the tests, as shown in Table 10. According to Table 10, it is clear that states 1 and 4 are those states where corrosion action has a low and high likelihood of occurring, respectively. Figure 9a and b show a graphical representation of the HCP data. Fig-

Table 10
Condition of Reinforcing Bars Based on HCP Values [32]

HCP values (Ag/AgCl electrode)	Termed State	Likely Corrosion Condition
> - 106 mV	State-1	Low (There is a greater than 90% probability that no reinforcement steel corrosion is occurring at the time of measurement)
- 106 mV to - 256 mV	State-2	Corrosion activity in that area is uncertain at the time of measurement
< - 256 mV	State-3	High (There is a greater than 90% probability that reinforcement steel corrosion is occurring at the time of measurement)
< - 406 mV	State-4	Severe Corrosion

ure 10a and b also display different states' percentage frequent occurrence distribution. Figure 9a and b show that different monitoring sessions did not reveal the same level of corrosion activity (states 1 to state 4) at the same spot. It implies that corrosion has a cyclical character, meaning that it can be active at one time and inactive at another at the same spot.

3.4. Recorded Temperature Profiles During Fire Testing

During the fire tests, the four MI-thermocouples that were installed in the fire furnace recorded the temperature of the furnace air. The average temperature profiles of the furnace while testing RC column specimens in the fire are shown in Figure 11a and b. During the tests, the furnace's temperature profile was intended to adhere to the ISO-834 standard fire curve. It was noted that during the fire testing of the HSC corroded specimen, enormous explosively spalled portions caused some leakage of fire, which can be seen in the furnace temperature profile of the HSC corroded column specimen (C60120C), as shown in Figure 11b, even though before the tests it was ensured there was no leakage of fire during the test by filling all possible gaps with glass wool material. Only the internal thermocouples placed at the concrete's core (T4) were found to be functional and recorded the temperature profiles during the fire testing of column specimens because other internal K-type thermocouples (T1, T2, T3, T5, T6, and T7) were found to be non-functioning due to corrosion. It might be because, in an RC element, a chloride attack occurs from the surface to the core, which has less of an impact on the metallic elements nearby the core. The internal core concrete temperature plots for the corroded columns, C30220C and C60120C, along with their respective non-corroded columns, C30330C and C60500C, can be observed in Figure. 12a and b. It can be noticed that the heat propagation inside the corroded columns was higher compared to their companion non-corroded specimens. This must be because the corrosion of the reinforcing bars in concrete puts tensile stresses on the nearby concrete, and because of the low tensile strength properties of concrete, cracks form that makes it easy for the heat flux to get transmitted inside the concrete [33, 34] (Q1). A corroded RC element comprises rust products (Iron oxide

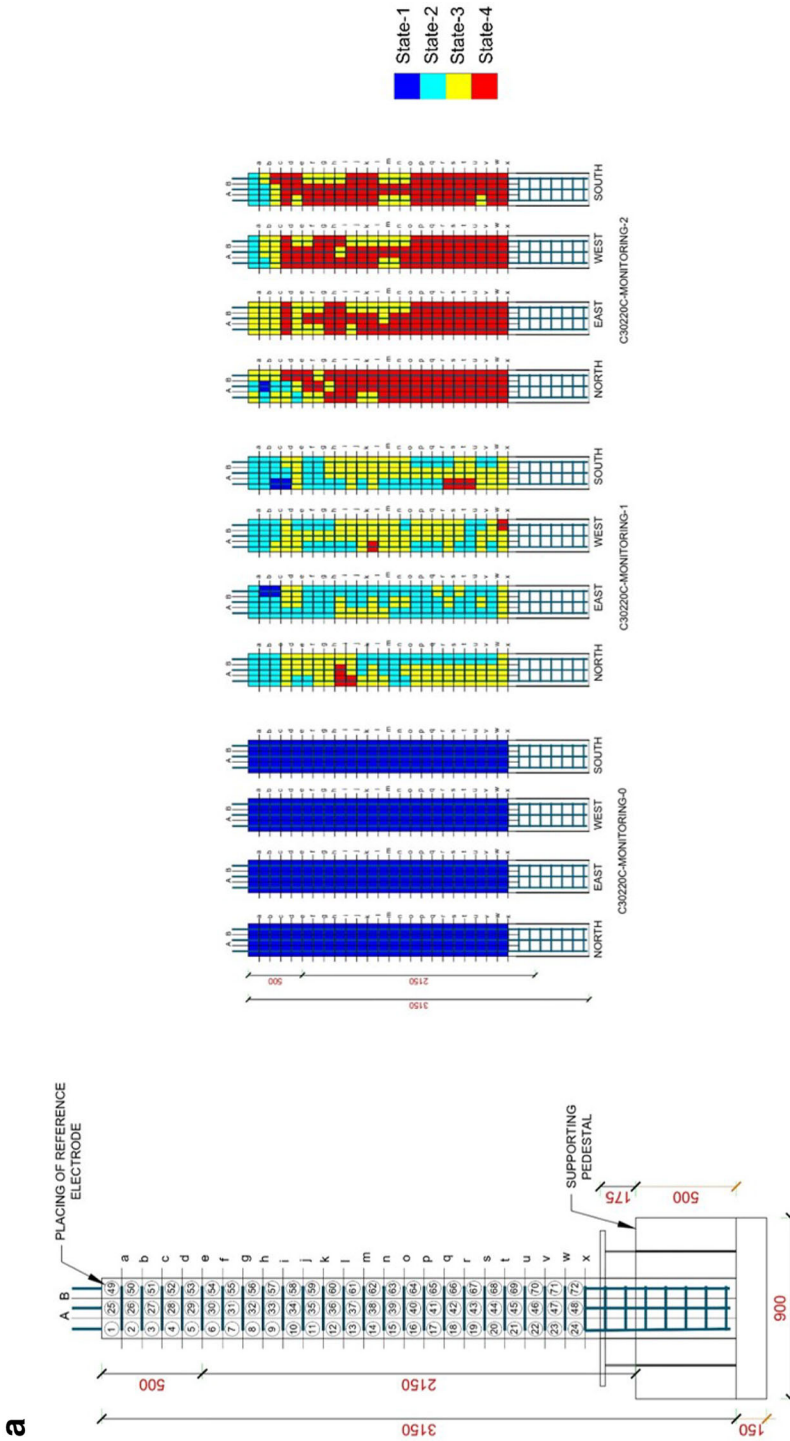


Figure 9. (a) Graphical representation of HCP data-C30220C (Corroded NSC). (b) Graphical representation of HCP data-C60120C (Corroded HSC).

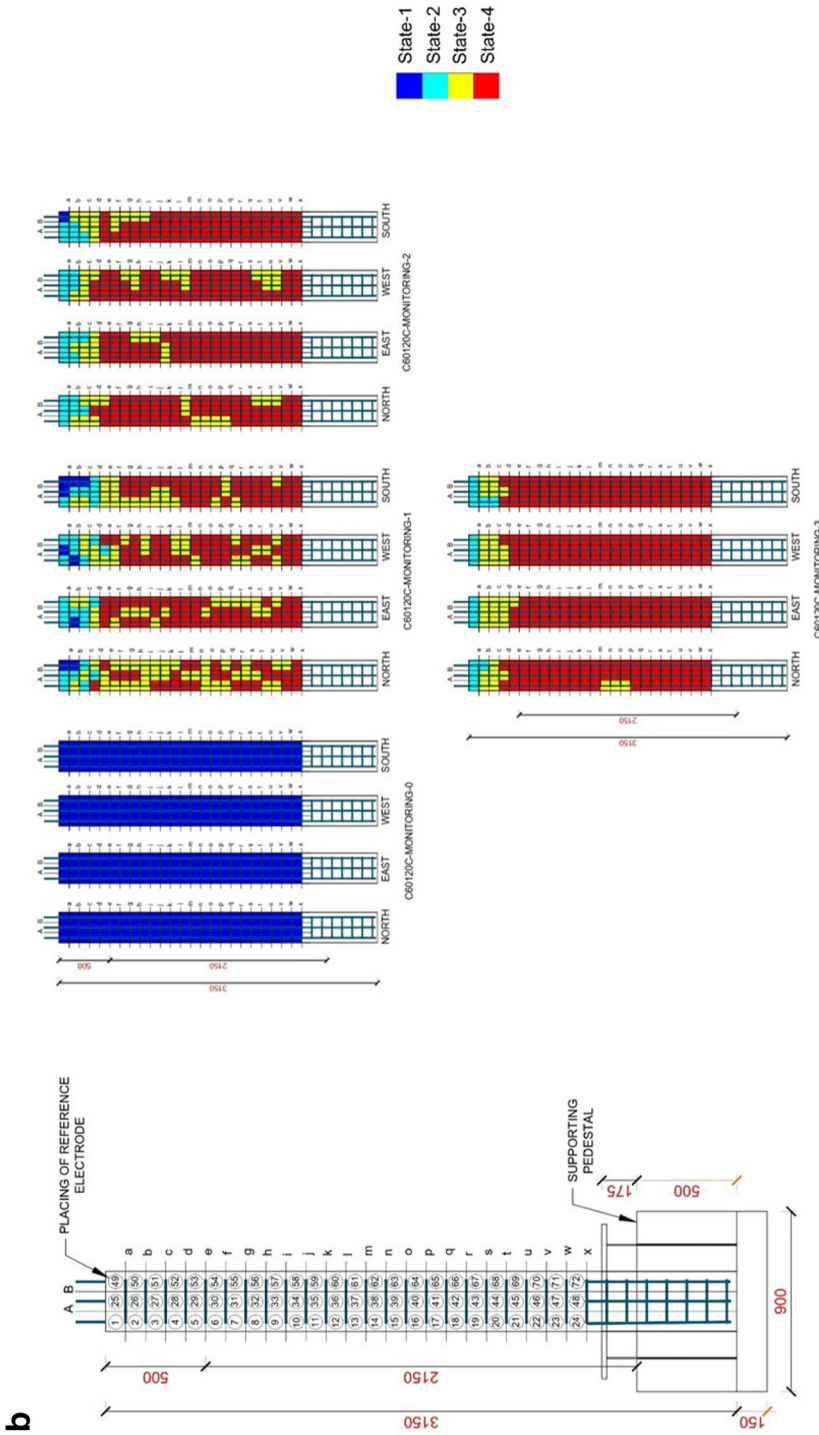


Figure 9. continued.

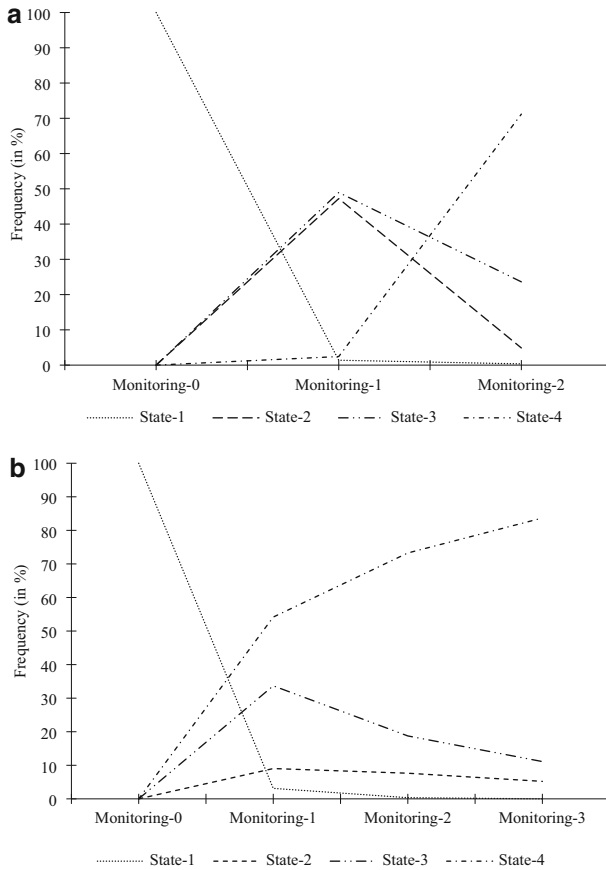


Figure 10. (a) Frequency occurrence distribution of C30220C (Corroded NSC). (b) Frequency occurrence distribution of C60120C (Corroded HSC).

and Ferro-ferric oxide), concrete, reinforcing elements, and air in the pores. The thermal conductivity of these rust products is much higher than the air [35]. Due to that, in the corroded RC structures, the cracks and the pores are now filled with rust products with much higher thermal conduction properties. It probably causes acceleration in the transmission of heat flux inside the corroded concrete element. This may be another reason for noting the core concrete temperature of corroded specimens on the higher side (Q2). On the other hand, these corrosion cracks might be helpful for the easier evacuation of vapours from the RC element in the event of a fire (V). The Q1, Q2 and V illustrations are shown in Figure 13 and discussed in Sect. 3.5.3 of this paper. Here, Figure 13 shows a general depiction of corroded concrete section.

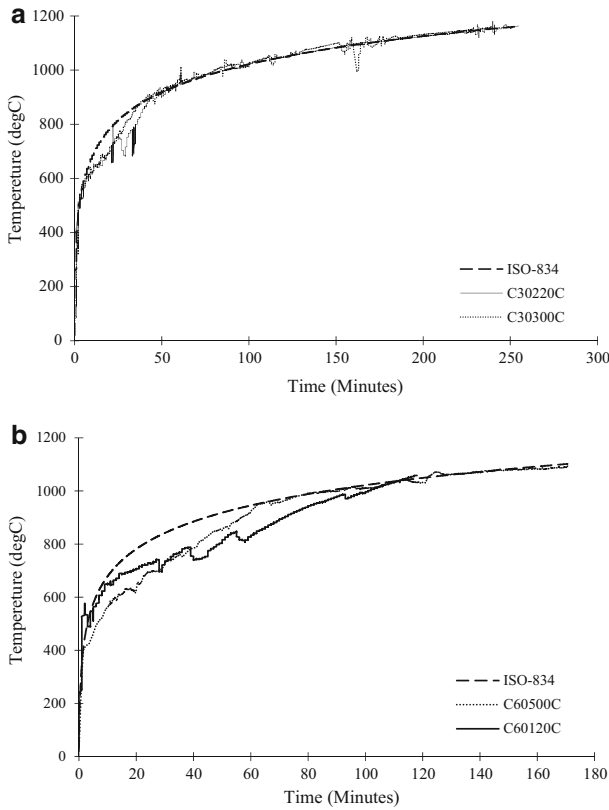


Figure 11. (a) Furnace temperature profiles of C30220C (Corroded NSC) and C30300C (Non-Corroded NSC) columns. (b) Furnace temperature profiles of C60120C (Corroded HSC) and C60500C (Non-Corroded HSC) columns.

3.5. Structural Responses of RC Columns During Fire Testing

3.5.1. Axial Deformations The measured axial deformations through LVDT V1 and V2 of all the columns during the event of the fire are mentioned in Figure 14a and b as a function of their respective fire exposure time. All the column specimens in the early fire stage expanded due to concrete and steel thermal expansion. Later, the contraction of the column specimens was seen as the result of a loss of strength in steel reinforcement and concrete. Even though the concrete is more fire-resistant than the steel reinforcement, the load on the concrete gradually rises as the steel reinforcement gradually starts to yield. At the same time, exposure to high temperatures affects the strength and stiffness of the concrete, ultimately leading to failure when the column cannot support the applied load. It can be seen that the thermal expansion of corroded specimens was found to be less than that of their companion non-corroded specimens; this can be attributed to the higher rebar temperature due to the presence of surface corrosion cracks present

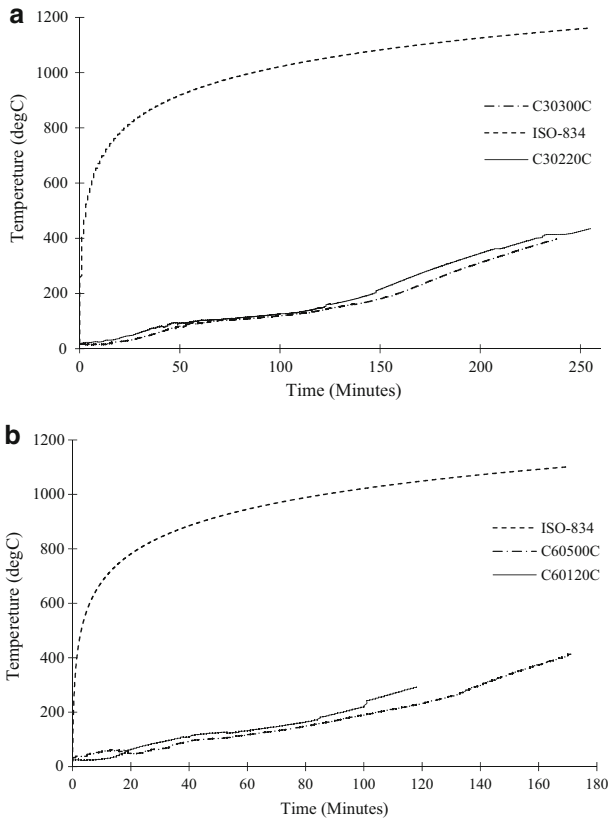
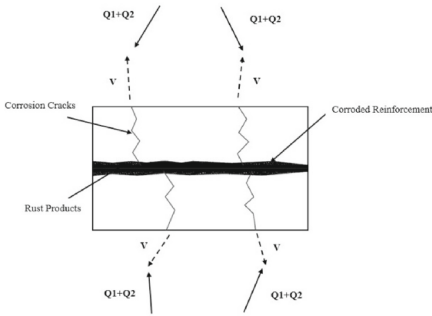


Figure 12. (a) Core concrete temperature profiles of C30300C (Non-Corroded NSC) and C30220C (Corroded NSC) columns (b) Core concrete temperature profiles of C60500C (Non-Corroded HSC) and C60120C (Corroded HSC) columns.

over the faces of the column specimens and also due to the faster degradation of strength and stiffness. The axial deformations in the corroded HSC specimen were found to be the function of severe explosive spalling occurring during the fire exposure. Although the applied load was concentric to the axis of the column cross-section, tilting of the specimens was observed, which can be seen in the differences between V1 and V2 values, as shown in Figure 14a and b. It must be because spalling occurs in a non-uniform manner during the fire event, which weakens one face of the column compared to the other. When the column could no longer sustain the applied load, a sudden drop in the load was observed, and failure occurred. The failure of the C60120C specimen was catastrophic, with the massive sound. It was found that the C60120C column suffered a shear failure. The failure of all the column specimens studied in this experimental investigation is shown in Figure 15.



Here,

Q_1 = Heat flux going inside the concrete due to the convenient passage through cracks.

Q_2 = Heat flux going inside the concrete due to the higher thermal conductivity of the rust products.

V = Vapors responsible for the spalling (S) are dissipating due to the convenient passage through cracks.

Figure 13. Heat propagation through corrosion cracks and relation with spalling: A general depiction of corroded concrete section.

3.5.2. Load Variation As mentioned earlier, a load of 33% axial capacity (P) of the respective RC column was applied before the start of the fire exposure. In the early phase of fire exposure, there is an expansion in the RC column; due to that, the acting load over the column increase. In the later stage, the acting load over the column reaches a certain peak value and after that, the load starts decreasing. This reduction in load occurs due to the degradation of strength and stiffness properties of both reinforcement and concrete, which cause a contraction in the column. The load variation during the fire test, as a function of their respective fire exposure time, is shown in Figure 16a and b. Specifically, during the fire tests of the corroded HSC column specimen, it was found that the load-carrying capacity was dependent on concrete spalling. At different severe spalling events, unexpected load drops (up to 2.75%) were noted during the fire testing of C60120C. The peak load attainment ability of the columns was also recorded. The C30220C and C30300C column specimens attained the peak at the values of 812.32 kN and 813.5 kN, respectively. Similarly, the C60120C and C60500C column specimens attained the peak at the value of 1092.4 kN and 1164 kN, respectively. The effect of corrosion over the peak load attainment can also be noticed significantly in the HSC columns. After reaching their respective peak loads, the acting load decreased, and after further fire exposure, the load returned to the initially applied load (P). The reduction in the load was found to be still continuous. At this time, the load was applied through the hydraulic jack, and it was tried to keep it equal to the initially applied load (P). After some time, the sudden load reduction was seen, and the RC column specimen could not sustain the load, and failure occurred. At the time of the failure of the C60120C column specimen, a sudden and massive load drop was observed in a catastrophic manner, which can be seen in the load profiles, as shown in Figure 16b.

3.5.3. Fire Resistance or Fire Ratings A comparison of the fire resistance of the four columns studied in this investigation is presented in Table 8. The fire exposure time to reach the failure is termed as fire resistance, and the failure is said to occur when the column in the event of fire exposure, can no longer sustain the applied load. Before the fire exposure, each column specimen was loaded with

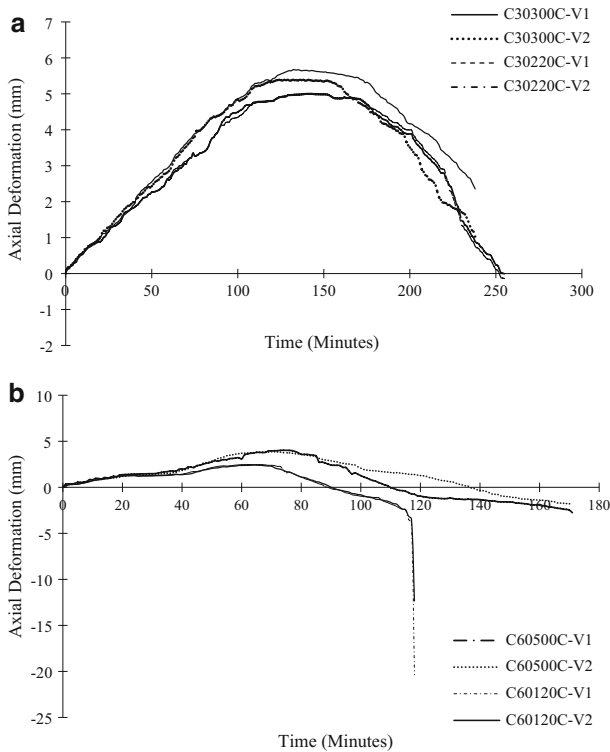


Figure 14. (a) Axial deformation as a function of time of C30300C (Non-Corroded NSC) and C30220C (Corroded NSC) columns. (b) Axial deformation as a function of time of C60500C (Non-Corroded HSC) and C60120C (Corroded HSC) columns.

33% of the axial load-carrying capacity (P). In the early stage of the fire, expansion of the columns was observed, which increased the load acting over the specimen. In later stages, the column contraction occurred, which reduced the acting load, and later, this load reached back to the actual applied load (P), as shown in Figure 16a and b. Now, the applied load was tried to maintain equal to P , but after some time, the column specimens were found unable to sustain the load (P), and this stage was called a failure of the column. The fire resistance of C30220C (255 min.) was found to be 6.7% greater than its companion non-corroded specimen C30300C (239 min.), and the fire resistance of C60120C (118 min.) was found to be decreased by 31.4% to its companion non-corroded specimen C60500C (171 min.). It should be noted here that Q_1 , Q_2 and V factors, illustrated in Figure 13, play a crucial role in deciding the fire rating of a corroded column. Here, Q_1 and Q_2 are the factors which are responsible for the early rise in rebar temperature inside the corroded specimen and hence also accountable for severe spalling, which further will cause the premature degradation of strength of the column in the fire event. On the other hand, V is the factor that mitigates the pore pressure

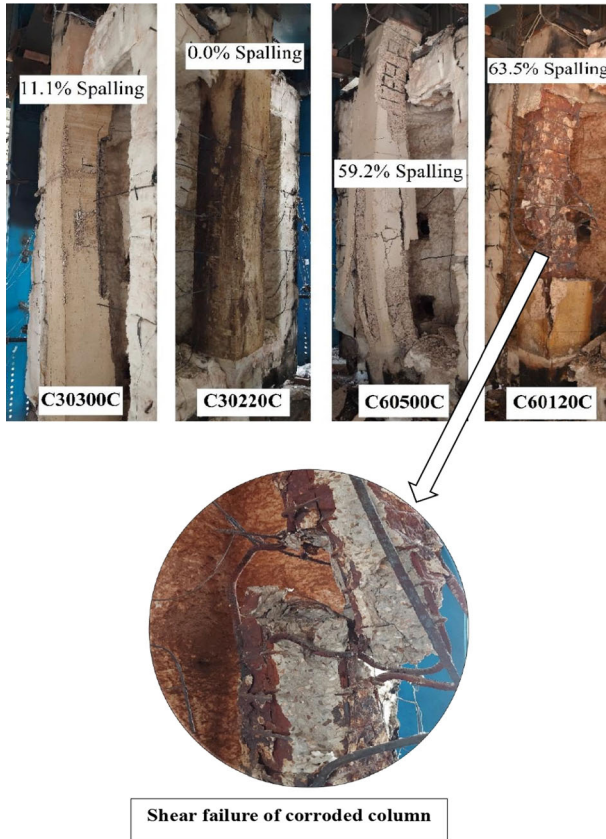


Figure 15. Failure of column specimens. Here, C30300C = Non-Corroded NSC; C30220C = Corroded NSC; C60500C = Non-Corroded HSC; C60120C = Corroded HSC.

inside the concrete during a fire event. Eventually, spalling might be minimized, which in turn can delay the process of the degradation of the strength of the column in the fire event. These Q1, Q2, and V events happen simultaneously during a fire event. It can be stated here that if the combined effect of Q1 and Q2 is greater than the individual effect of V, then a loss in the fire ratings will be observed, as found with the C60120C column specimen. On the other hand, if the corrosion degree is less, then the individual effect of V might be greater than the combined effect of Q1 and Q2, and then the corroded columns may have significantly reduced spalling and eventually might have higher fire ratings than their non-corroded specimens, as in C30220C, the amount of spalling reduced to 0.0% and there is a slight enhancement in the fire ratings when compared to its companion non-corroded column specimen, C30300C.

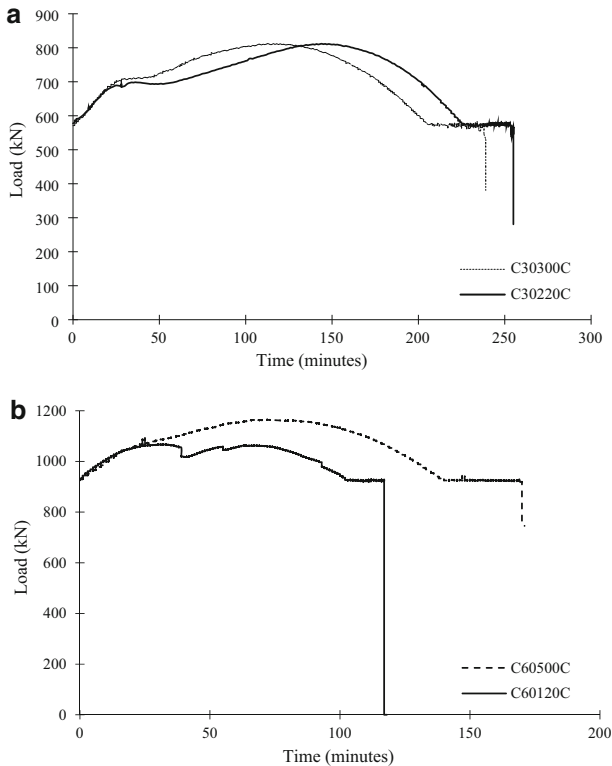


Figure 16. (a) Load variation as a function of time of C30300C and C30220C columns. (b) Load variation as a function of time of C60500C and C60120C columns.

3.5.4. Lateral Deformations Lateral deformation responses of the column specimens during the fire exposure time were measured, and their plots at various time intervals of 0.0 T, 0.125 T, to 1.0 T are given in Figure 17a to d. Here, T is that particular column specimen's total fire exposure time or fire resistance. During the early stage of fire exposure, the column undergoes axial expansion. In the later stage, when the degradation in the strength and stiffness of the concrete and rebars starts, the contraction of the column occurs, as already shown in Figure 14a and b. The time of this initiation of degradation was noted during the fire test and termed as Critical Time (CT). The lateral deformation plots of the column specimens at this time of fire exposure are also plotted in Figure 17a to d. The critical time (CT) can also be defined as the time after which the residual strength of the column plays a vital role in sustaining the loads during the fire exposure. Here, critical time is expressed in a multiplier of T, the total fire exposure time of that particular column specimen. The critical time of C30200C was 0.56 times its total exposure time ($T = 255$ min), and for its companion non-corroded specimen, i.e., C30300C, it was found to be 0.55 times its total fire exposure time ($T = 239$ min). On the other hand, the critical time of C60120C was 0.54

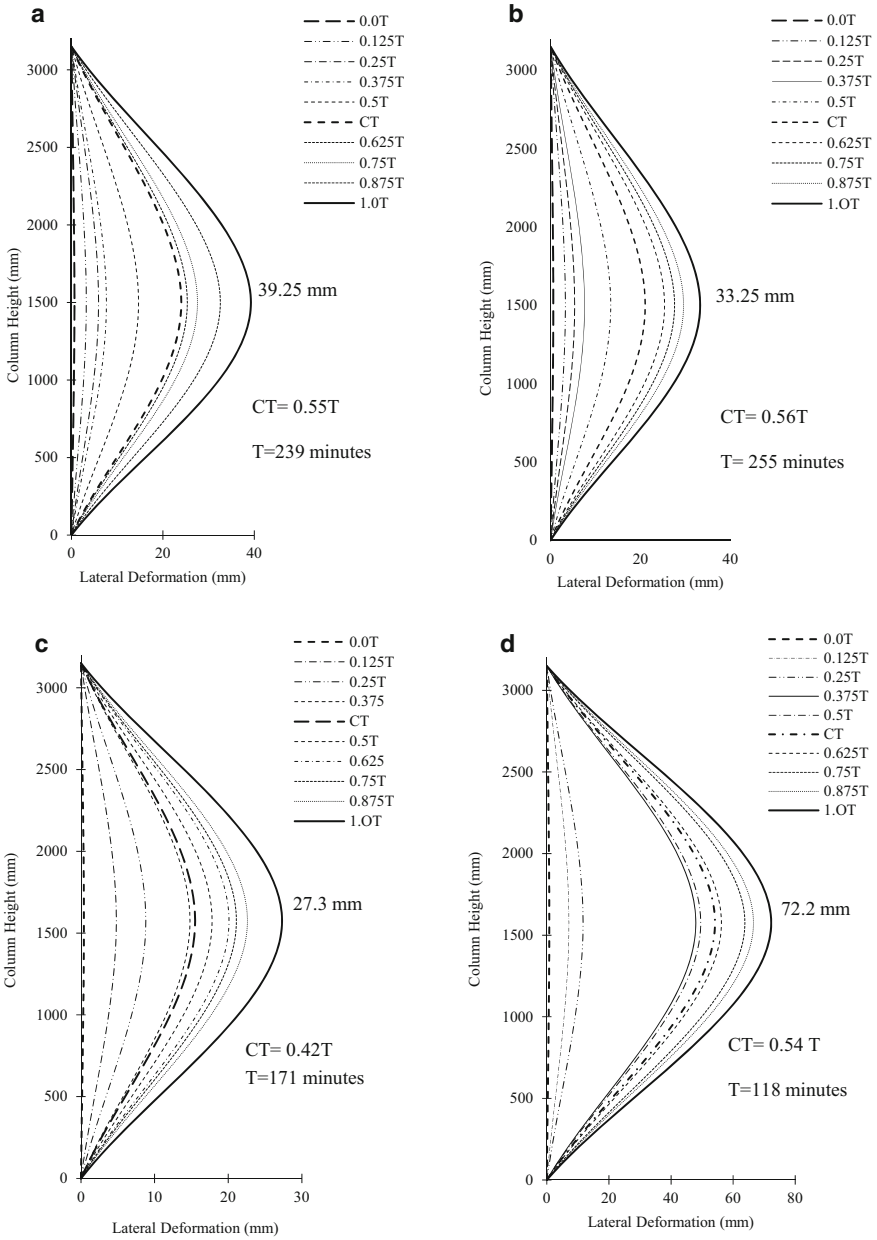


Figure 17. (a) Lateral deformation of C30300C (Non-Corroded NSC). (b) Lateral deformation of C30220C (Corroded NSC). (c) Lateral deformation of C60500C (Non-Corroded HSC). (d) Lateral deformation of C60120C (Corroded HSC).

times its total exposure time ($T = 118$ min), and for its companion non-corroded specimen, i.e., C60500C, it was found to be 0.42 times its total fire exposure time ($T = 171$ min). It can also be admitted here that higher the critical time, lesser the time left with the specimen to sustain the load before the failure. Corroded columns exhibited higher critical time, which signifies that the degradation in the strength and stiffness of the RC Column is faster after progressing to their respective critical time. The more significant lateral deformations were observed in the corroded specimen after their respective critical times, which inferred that the corroded specimens degraded faster in the later stages of fire exposure. It can also be noted from Figure 17a and b that a slightly lesser lateral deformation of C30220C was recorded compared to its companion non-corroded specimen, C30300C. It must be because corrosion cracks in this corroded specimen helped for easier evacuation of vapours from inside. This minimized the spalling during fire exposure and reduced the lateral deflections. The total fire exposure time of C30220C was increased by 6.7%, with a reduction of 15.2% in final lateral deflection, compared to its non-corroded companion, C30300C. In contrast, in C60300C, the total fire exposure time of C60120C dropped by 31.3%, with a significant increase of 164.46% in final lateral deflection compared to its non-corroded companion, C60500C, as shown in Figure 17c and d. Such high lateral deflections in the HSC corroded specimen must be due to the sloughing-off of loose cover concrete in the early phases (between $0.25 T$ to $0.375 T$) of their respective fire exposure, which can be seen in Figure 17d.

3.6. Spalling Behaviour of Columns During Fire Testing

After the fire test, the furnace was opened on the next day, and spalled areas of the tested columns were measured. The spalling areas were measured on all the faces of the columns and represented in the cumulative form in Table 8. During the tests, the concrete made noisy breaking and bursting noises that were signs of severe block spalling and chip splitting. These noises were thought to be signs of concrete spalling (S) in columns. This observation noted that spalling typically started around 38 min for C30300C, 11 min for C60120C, and 14 min for C60500C of the fire tests. It can also be seen that completely no spalling was observed in the C30220C column. It must be because, at a low percentage of corrosion, the corrosion cracks act as the convenient medium to come out of the concrete element for the vapours responsible for spalling, as mentioned earlier in Sect. 3.5.3, but as spalling is a complex occurrence, making it challenging to derive conclusive statements solely based on corrosion, detailed research is necessary in regards to this.

It can also be noted that the HSC corroded column, C60120C, exhibited early and severe spalling during the fire testing. It must be because, due to corrosion, the bond between the reinforcing elements and cover concrete has been significantly lost. And hence, the early and severe spalling of cover concrete exposed the reinforcing elements directly to the fire, and then rapid degradation in the strength eventually caused the earlier failure of the HSC corroded column. It can be said that spalling in a corroded column might depend on three factors, Q1, Q2 and V.

The details of Q1, Q2, and V are already mentioned in Figure 13. The following relations might be derived to express the relations between the spalling (S) and these factors (Q1, Q2, and V) in a corroded column.

$$S = f(Q1, Q2, V)$$

$$S \propto Q1, S \propto Q2, S \propto \frac{1}{V}$$

$$S = \frac{K(Q1 + Q2)}{V}, \text{ Here, } K = \text{Aconstant.}$$

If, $Q1 + Q2 > V$, then $S \uparrow$

And, if $Q1 + Q2 < V$, then $S \downarrow$

4. Conclusion

The main objective of this study was to examine the influence of corrosion on the fire performance of RC columns. The following conclusions may be drawn from this study:

- Corrosion of reinforcement affects the strength and stiffness properties of RC columns. With a corrosion degree of 12.29%, the behavior of the corroded NSC column shows a slight improvement when exposed to fire, indicating the need for further detailed research in this area. On the contrary, at a 15.38% degree of corrosion, there was a significant loss in the fire resistance of HSC columns.
- Due to the surface corrosion cracks and higher thermal conductivity of rust products, the heat flux quickly penetrates the core portion of the concrete section compared to its companion non-corroded specimen, which eventually increases the initial rise of temperatures in the rebars.
- The presence of corrosion cracks in the corroded specimen caused the earlier temperature rise in the corroded specimens' rebars. Due to that, a comparable less axial expansion of the corroded columns was observed in the early stages of fire exposure.
- At the low percentage of corrosion in the normal strength concrete column, the corrosion cracks may be vital in quickly evacuating the vapours from the RC elements. They can cause a significant reduction in the spalling, which eventually can even enhance the fire performance, indicating the need for further detailed research in this area.

- Spalling of concrete must play an essential role in the lateral deformation characteristics of the column specimen in the event of fire exposure. As spalling was prevented by corrosion cracks in the NSC column, slightly lesser lateral deformation was observed compared to its companion non-corroded specimen.
- The time of the fire exposure at which the column's degradation starts was termed as critical time (CT). The HSC corroded column specimen exhibits an enormous lateral deformation response in the later stages of fire exposure after advancing to its respective critical time (CT).
- There are consequences of severe concrete spalling over the load progression during the fire test.
- HSC corroded specimen undergoes severe spalling during its fire exposure which eventually causes the earlier loss of strength and stiffness properties of concrete and rebar.

Acknowledgements

The Department of Science and Technology (DST), Government of India, financially supported this experimental investigation program. The authors wish to thank for that.

Declarations

Conflict of interest The authors whose names are listed immediately below certify that they have **NO** affiliations with or involvement in any organisation or entity with any financial interest (such as honoraria; educational grants; participation in speakers' bureaus; membership, employment, consultancies, stock ownership, or other equity interest; and expert testimony or patent-licensing arrangements), or non-financial interest (such as personal or professional relationships, affiliations, knowledge or beliefs) in the subject matter or materials discussed in this manuscript.

References

1. Zhang W, Song X, Gu X, Li S (2012) Tensile and fatigue behavior of corroded rebars. *Constr Build Mater* 34:409–417
2. Suda K, Misra S, Motohashi K (1993) Corrosion products of reinforcing bars embedded in concrete. *Corros Sci* 35(5–8):1543–1549
3. Fang C, Lundgren K, Chen L, Zhu C (2004) Corrosion influence on bond in reinforced concrete. *Cem Concr Res* 34(11):2159–2167
4. Coccia S, Imperatore S, Rinaldi Z (2016) Influence of corrosion on the bond strength of steel rebars in concrete. *Mater Struct* 49(1):537–551
5. Lundgren K (2007) Effect of corrosion on the bond between steel and concrete: an overview. *Mag Concr Res* 59(6):447–461

6. Rodriguez J, Ortega LM, Casal J (1997) Load carrying capacity of concrete structures with corroded reinforcement. *Constr Build Mater* 11(4):239–248
7. Rajput AS, Sharma UK (2018) Corroded reinforced concrete columns under simulated seismic loading. *Eng Struct* 171:453–463
8. Xia J, Jin WL, Li LY (2016) Performance of corroded reinforced concrete columns under the action of eccentric loads. *J Mater Civ Eng* 28(1):04015087
9. Ou YC, Nguyen ND (2016) Influences of location of reinforcement corrosion on seismic performance of corroded reinforced concrete beams. *Eng Struct* 126:210–223
10. Liu X, Jiang H, He L (2017) Experimental investigation on seismic performance of corroded reinforced concrete moment-resisting frames. *Eng Struct* 153:639–652
11. U.S. Fire Administration (2018) Non-residential building fire trends (2007–2016), Emmitsburg
12. Kodur V (2014) Properties of concrete at elevated temperatures. *International Scholarly Research Notices* . <https://doi.org/10.1155/2014/468510>
13. Wu H, Lin X, Zhou A (2020) A review of mechanical properties of fibre reinforced concrete at elevated temperatures. *Cem Concr Res* 135:106117
14. Cheng FP, Kodur VKR, Wang TC (2004) Stress-strain curves for high-strength concrete at elevated temperatures. *J Mater Civ Eng* 16(1):84–90
15. Youssef MA, Moftah M (2007) General stress-strain relationship for concrete at elevated temperatures. *Eng Struct* 29(10):2618–2634
16. Morley PD, Royles R (1983) Response of the bond in reinforced concrete to high temperatures. *Mag Concr Res* 35(123):67–74
17. Morley PD, Royles R (1980) The influence of high temperature on the bond in reinforced concrete. *Fire Saf J* 2(4):243–255
18. IS 3809 (1979) Fire resistance test for structures
19. Shah AH, Sharma UK (2017) Fire resistance and spalling performance of confined concrete columns. *Constr Build Mater* 156:161–174
20. Franssen JM, Dotreppe JC (2003) Fire tests and calculation methods for circular concrete columns. *Fire Technol* 39(1):89–97
21. Raut NK, Kodur VKR (2011) Response of high-strength concrete columns under design fire exposure. *J Struct Eng* 137(1):69–79
22. Rodrigues JPC, Laím L, Correia AM (2010) Behaviour of fiber reinforced concrete columns in fire. *Compos Struct* 92(5):1263–1268
23. Buch SH, Sharma UK (2019) Fire resistance of eccentrically loaded reinforced concrete columns. *Fire Technol* 55:1517–1552
24. EN 1992–1–2 (1992) Eurocode 2: Design of concrete structures - Part 1–2: General rules - Structural fire design
25. C. S. Standards Association of Australia. Committee BD-002, Concrete structures : AS 3600–2009
26. Yang O, Zhang B, Yan G, Chen J (2018) Bond performance between slightly corroded steel bar and concrete after exposure to high temperature. *J Struct Eng* 144(11):04018209
27. Tariq F, Bhargava P (2021) Flexural behaviour of corroded RC beams exposed to fire. *Structures*, vol 33. Elsevier, Amsterdam, pp 1366–1375
28. Ba G, Miao J, Zhang W, Liu J (2019) Influence of reinforcement corrosion on fire performance of reinforced concrete beams. *Constr Build Mater* 213:738–747
29. IS/ISO 834–1 (1999) Fire-Resistance Tests — Elements of Building Construction: Part 1 General Requirements
30. IS 456 (2000) Plain and Reinforced Concrete - Code of Practice

31. (Reapproved:2011) A-03 (2016) Standard practice for preparing, cleaning, and evaluating corrosion test. ASTM G1-03 03:1-9. <https://doi.org/10.1520/G0001-03R11.2>
32. I. Standard, Hardened Concrete-Methods of Test Part 5 Non-Destructive Testing Section Half-Cell Potentials of Uncoated Reinforcing Steel in Concrete, 2021
33. Ba G, Miao J, Zhang W, Liu C (2016) Influence of cracking on heat propagation in reinforced concrete structures. *J Struct Eng* 142(7):04016035
34. Wu B, Xiong W, Wen B (2014) Thermal fields of cracked concrete members in fire. *Fire Saf J* 66:15-24
35. Takeda M, Onishi T, Nakakubo S, Fujimoto S (2009) Physical properties of iron-oxide scales on Si-containing steels at high temperature. *Mater Trans* 50(9):2242-2246

Publisher's Note Springer Nature remains neutral with regard to jurisdictional claims in published maps and institutional affiliations.

Springer Nature or its licensor (e.g. a society or other partner) holds exclusive rights to this article under a publishing agreement with the author(s) or other rightsholder(s); author self-archiving of the accepted manuscript version of this article is solely governed by the terms of such publishing agreement and applicable law.